Since January 2020 Elsevier has created a COVID-19 resource centre with free information in English and Mandarin on the novel coronavirus COVID-19. The COVID-19 resource centre is hosted on Elsevier Connect, the company's public news and information website.

Virology 478 (2015) 75–85

Contents lists available at ScienceDirect

Virology

journal homepage: www.elsevier.com/locate/yviro

Coronavirus envelope (E) protein remains at the site of assembly

Pavithra Venkatagopalan [a,b,d], Sasha M. Daskalova [a,c], Lisa A. Lopez [a,b,e], Kelly A. Dolezal [a,b,d], Brenda G. Hogue [a,b,*]

[a] The Biodesign Institute, Center for Infectious Diseases and Vaccinology, Arizona State University, Tempe, AZ 85287-5401, United States
[b] School of Life Sciences, Arizona State University, Tempe, AZ 85287-5401, United States
[c] Department of Biochemistry and Chemistry, Arizona State University, Tempe, AZ 85287-5401, United States
[d] Microbiology Graduate Program, Arizona State University, Tempe, AZ 85287-5401, United States
[e] Molecular and Cellular Biology Graduate Program, Arizona State University, Tempe, AZ 85287-5401, United States

ARTICLE INFO

Article history:
Received 4 September 2014
Returned to author for revisions
19 September 2014
Accepted 4 February 2015
Available online 27 February 2015

Keywords:
Coronavirus
Envelope protein
Protein transport/localization
Virus assembly
Live-cell imaging
FRAP
CLEM

ABSTRACT

Coronaviruses (CoVs) assemble at endoplasmic reticulum Golgi intermediate compartment (ERGIC) membranes and egress from cells in cargo vesicles. Only a few molecules of the envelope (E) protein are assembled into virions. The role of E in morphogenesis is not fully understood. The cellular localization and dynamics of mouse hepatitis CoV A59 (MHV) E protein were investigated to further understanding of its role during infection. E protein localized in the ERGIC and Golgi with the amino and carboxy termini in the lumen and cytoplasm, respectively. E protein does not traffic to the cell surface. MHV was genetically engineered with a tetracysteine tag at the carboxy end of E. Fluorescence recovery after photobleaching (FRAP) showed that E is mobile in ERGIC/Golgi membranes. Correlative light electron microscopy (CLEM) confirmed the presence of E in Golgi cisternae. The results provide strong support that E proteins carry out their function(s) at the site of budding/assembly.

Introduction

Coronavirus (CoV) envelope (E) proteins play multiple roles during infection, including virus morphogenesis and, at least in the case of severe acute respiratory syndrome (SARS) CoV, pathogenesis. E proteins are small (74-109 amino acids) hydrophobic viroporins (Hogue and Machamer, 2008; Ruch and Machamer, 2012a; Wilson et al., 2006, 2004). The proteins consist of two distinct structural domains, a longer than typical hydrophobic domain and a charged cytoplasmic tail. E proteins from across the virus family exhibit amino acid sequence variability. However, E proteins from other coronaviruses can replace MHV E (Kuo et al., 2007). This suggests that the proteins provide a common function that is interchangeable among the viruses, but this has not been tested yet for other CoVs. Surprisingly, a truncated variant of the M protein was shown to also enhance the growth of MHV lacking the E gene (Kuo and Masters, 2010). Even though the effect on growth was positive, infectious virus titers in the presence of the M variant were 100-fold lower than for wild-type MHV and the mutant viruses appeared to be less stable.

CoVs assemble at intracellular membranes in the ERGIC compartment where they bud into the lumen and are subsequently transported out of the cell by exocytosis in cargo vesicles (Krijnse-Locker et al., 1994; Tooze and Tooze, 1985). For all CoVs the membrane (M) and spike (S) proteins constitute the majority of the protein that is incorporated into the viral envelope, whereas only a few molecules of the E protein are present (Godet et al., 1992; Liu and Inglis, 1991; Yu et al., 1994). The envelope surrounds the ~30 kb single-stranded, positive sense RNA genome that is encapsidated by the phosphorylated nucleocapsid (N) protein as a helical nucleocapsid.

The role of E proteins in assembly and egress is not fully understood. The absolute requirement for E during virus morphogenesis varies depending on the virus genus. The E protein is not absolutely essential for β genus MHV, but virus production is significantly compromised (1000-fold) in the absence of the protein, thus indicating that the protein plays an important role during morphogenesis (Kuo and Masters, 2003). Deletion of the E proteins from the α genus transmissible gastroenteritis virus (TGEV) results in replication-competent, but propagation-defective viruses, as is the case with the β genus Middle Eastern Syndrome virus (MERS) (Curtis et al., 2002) (Almazan et al., 2013; Ortego et al., 2007, 2002). SARS CoV, also a member of β genus, exhibited only a 20- to 200-fold reduction in virus output in the absence of E that was dependent on the cell type used for infection (DeDiego et al., 2007, 2014, 2008).

* Correspondence to: The Biodesign Institute, Arizona State University, PO Box 875401, Tempe, AZ 85287-5401, United States. Tel.: +1 480 965 9478; fax: +1 480 727 7615.
E-mail address: Brenda.Hogue@asu.edu (B.G. Hogue).

http://dx.doi.org/10.1016/j.virol.2015.02.005
0042-6822/

E proteins also oligomerize and form ion channels (Wilson et al., 2006, 2004). The relevance of ion channel activity in morphogenesis is still not clear, but recent studies have shown that SARS-CoV E protein is a virulence factor that influences pathogenesis in a mouse model (DeDiego et al., 2007, 2014, 2008; Regla-Nava et al., 2015). It remains to be shown if other CoV proteins are contributors to pathogenesis.

Knowledge about its cellular localization is important to fully understand the roles that E proteins play during infection, whether in morphogenesis or pathogensis. To help further our understanding of the mechanistic role(s) in virus assembly and egress or other roles that CoV E proteins play, we carried out a study to precisely define the cellular localization and expression dynamics of E from MHV A59, one of the long-standing prototype members of the β genus. We show that MHV E localizes in both the ERGIC and Golgi and that the protein does not traffic to the cell surface during infection. The protein is oriented with its carboxy end on the cytoplasmic side of the membranes and the amino end on the luminal side, as was suggested some years ago. To investigate the kinetics of E trafficking, MHV was genetically engineered with a tetracysteine (TC) tag appended to the carboxy end of the protein to allow for real-time imaging during infection. When monitored in real-time, the E protein was found to be mobile in ER/ERGIC membranes. Additionally, using correlative light electron microscopy E was visualized directly in Golgi stacks. The results provide further support showing that CoV E proteins carry out their functions at intracellular membranes where virus assembly occurs. This is the first report to describe live-cell imaging of a CoV E protein, which expands opportunities to analyze the interplay between E proteins and their host cells to help further understanding of the functions they provide during morphogenesis and pathogenesis.

Results

MHV-A59 E localizes in the ERGIC and Golgi

To identify the cellular localization of E protein within infected cells, 17Cl1 mouse cells were infected with wild-type MHV A59. The E protein exhibited compact localization adjacent to the nucleus as early as 6 h p.i. that did not overlap with the ER marker, protein disulfide isomerase (PDI) (Fig. 1A). Instead, the protein co-localized with markers of both the ERGIC and Golgi structures (middle two panels). Cells dual-labeled for the M and E proteins exhibited complete overlap of the signals (lower panels), indicative of colocalization.

To determine the distribution of the E protein in the Golgi, colocalization with *cis*-Golgi GM-130, medial-Golgi Mann-II and *trans*-Golgi p230 was examined (Fig. 1B). E colocalized most extensively with the *cis*- and medial-Golgi markers and less so with the trans-Golgi marker p230. Altogether, the results clearly define MHV E localization during infection in both the ERGIC and Golgi, with it being concentrated primarily in the *cis* and medial regions of the latter.

MHV E does not traffic to the cell surface

To further address localization and trafficking of MHV E, protein expression was examined in cells during a time course following infection. The S and M proteins were analyzed in parallel as controls (data not shown). The S protein is known to colocalize with M at the site of assembly, but it is also transported to the cell surface (Heald-Sargent and Gallagher, 2012). The M protein localizes in the Golgi (Corse and Machamer, 2002; Klumperman et al., 1994). At 8 h p.i. the E and M proteins continued to colocalize as was observed at 6 h p.i. (Fig. 2). By 12 h p.i. the M protein was localized in areas of the cell distant from the ERGIC/Golgi region, whereas the E protein remained localized at the perinuclear site. Additionally, E did not localize with the M or S proteins distant to the perinuclear sites when all three proteins were analyzed at 12 h p.i. (data not shown). At 16 h p.i., and more prominently at 24 h p.i., a large portion of the M protein was visualized throughout the cytoplasm, presumably as virus output increased and virions are being transported out of the cell. In contrast, at the late time points E continued to remain localized primarily in the ERGIC/Golgi region. Only a few small punctate dots were seen outside of these regions, presumably due to the extensive fusion that is

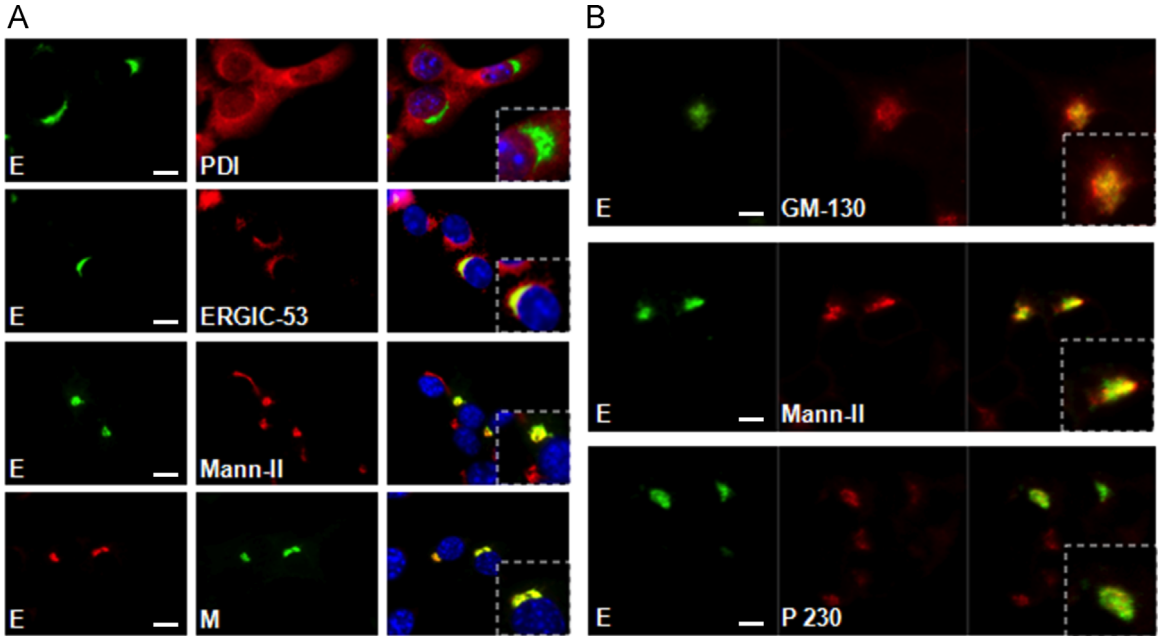

Fig. 1. MHV E localizes in the ERGIC and Golgi. Mouse 17Cl1 cells were infected with MHV A59 at a MOI of 1 and analyzed at 6 h p.i. (A) Cells were processed for dual-label immunofluorescence detection of E and protein disulfide isomerase (PDI), ERGIC-53, or mannosidase II (Mann-II), as ER, ERGIC, and Golgi markers, respectively. The bottom panels were probed for M and E proteins using rabbit polyclonal anti-E 9410 and mouse monoclonal J1.3 and J2.7 antibodies, respectively. Alexa-Fluor tagged secondary antibodies were used to counter stain the primary antibodies. Merged images are shown in the far right column, with enlarged insets of selected cells. Epifluorescence images were taken using a 60 × objective. (B) Cells were processed for dual-label immunofluorescence detection using antibodies specific for E (9410) and cis Golgi GM 130, medial Golgi Mann-II or trans Golgi p230. Confocal images were taken with a 100 × objective. Merged images are shown in the far right column, with enlarged insets of selected cells. Scale bar, 5 μm (A, B).

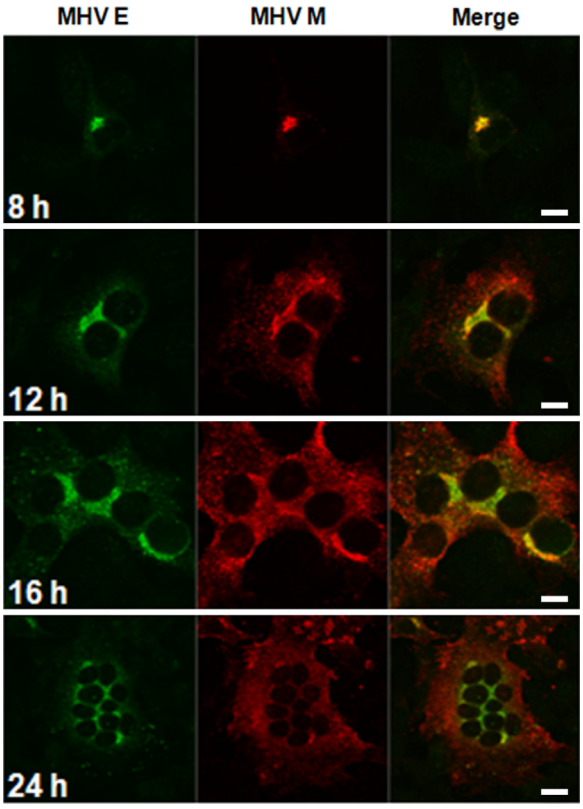

Fig. 2. MHV E does not traffic beyond the site of assembly. 17Cl1 mouse cells were infected with MHV A59 at a MOI of 1 and fixed at the specified times after infection. Indirect immunofluorescence was used to probe for E (green) and M (red) proteins. In the merged images yellow signifies where the two proteins colocalize at different times during infection. Confocal images were taken with a 63 × objective. Scale bars: 10 μm (8, 12, and 16 h p.i.) and 20 μm (24 h p.i.).

characteristic of MHV A59 infected cells at late times after infection (Heald-Sargent and Gallagher, 2012). These results indicate that the E and M proteins colocalize at the ERGIC/Golgi assembly site early during infection; the E proteins remain there at later times as virions and S traffic toward the cell surface.

Previous reports suggested that coronavirus E proteins are expressed on the cell surface during infection (Smith et al., 1990; Godet et al., 1992; Yu et al., 1994). To further examine this, cells infected or transiently expressing E were analyzed for surface expression (Fig. 3). The S and M proteins were monitored in parallel as positive and negative controls, respectively, for surface expression. Two approaches were used to monitor surface expression. First, 17Cl1 cells were infected with wild-type MHV A59 and cell surface proteins were biotinylated at 16 and 18 h p.i. (Fig. 3A). Biotinylated surface proteins were isolated with streptavidin agarose beads. Both surface and intracellular fractions were then analyzed by Western blotting for the viral proteins. As expected, the S protein was detected in both the intracellular (I) and surface (S) fractions, characteristic of a protein that transports through the exocytic pathway (Fig. 3A, top). The M protein was also detected in both fractions at later time points (data not shown), whereas the E protein was detected only in the intracellular fraction at all times, indicating that it was not accessible on the cell surface for biotinylation (Fig. 5A, lower panel).

Surface localization of E proteins was also analyzed by immunoflouresence (Fig. 3B). 17Cl1 cells were infected with MHV and probed with specific antibodies for S, M or E proteins after cells were permeabilized with digitonin or Triton X-100 (TX-100) to allow detection of either cytoplasmic epitopes only (digitonin) or the detection of both luminal and cytoplasmic epitopes (TX-100). The amino end of the M protein (luminal side) was recognized by monoclonal antibody J1.3 in the perinuclear region after cells were permeabilized with TX-100, but not with digitonin, consistent with the orientation of the protein at intracellular membranes and its known localization (Fig. 3B, middle images) (Klumperman et al., 1994; Locker et al., 1992). The S protein was detected inside the cell and also on the cell surface (Fig. 3B, top images). The E protein was detected in the perinuclear region in both TX-100 and digitonin treated cells when probed with antibody 9410 that recognizes the carboxy terminus (Fig. 3B, bottom images). This is consistent with the carboxy tail of the E protein being located on the cytoplasmic side of internal membranes, as suggested previously (Raamsman et al., 2000). No signal was detected on the surface of nonpermeabilized cells with the 9410 antibody (Fig. 3C, lower images). This indicates that the carboxy end of the E protein is not exposed on the cell surface.

Since antibodies that recognize the amino end of E were not available, we made use of a construct with a Strep tag appended on the amino end of the E protein to help further determine if it traffics to the cell surface (Fig. 3C). VLPs can be assembled with the Strep-tagged E which is coexpressed with M (data not shown), thus we reasoned that it would provide a relevant assessment for whether the amino end is accessible at the cell surface. BHK-21 cells were transfected with the pCAGGS vector containing the Strep-tagged E gene. The amino end of the E protein was detected by an antibody that recognizes the Strep tag, but only when cells were permeablized with TX-100 and not when permeabilized with digitonin (Fig. 3C, bottom images). This indicates that the amino end is located inside the lumen and not exposed on the cytoplasmic side of the ERGIC/Golgi membranes. In parallel, a signal was observed in both cases with the 9410 antibody, indicating that the carboxy end of E is located in the cytoplasm. No signal was observed with either antibody when cells were not permeablized, which shows that indeed the amino end is also not exposed on the cell surface.

Generation of MHV with a tetracysteine (TC)-tagged E protein

To investigate the dynamics of E expression in live cells, we constructed a recombinant E protein with a TC tag (CCPGCC) appended at the carboxy end. It was designated as pCAGGS E-TC (Fig. 4). TC tags form hairpin structures that bind small, membrane-permeable fluorescein derivatives such as the fluorescein arsenical hairpin binder Lumio™ Green (FlAsH™) or a variant, resorufin arsenical hairpin binder Lumio™ Red (ReAsH™), a red-shift analog (Gaietta et al., 2002; Griffin et al., 1998). The biarsenicals are fluorescent when they bind to TC tags. We initially confirmed that the tagged E could support VLP formation when the M and TC-tagged E proteins were co-expressed in 293T cells (data not shown). We also confirmed that the TC-tagged E protein localized correctly in the ERGIC/Golgi (Fig. 4). It was noted that the signal from recognition of the TC tag by either Lumio™ Green or Red is lower than what is achieved by the high-affinity 9410 antibody that recognizes the carboxy end of the E protein. However, the signal and resolution achieved for the TC tag was strong enough to allow clear localization and monitoring of the protein.

Having determined that the tag does not interfere with the protein's localization and that it supports VLP production, we then constructed a recombinant MHV A59 with the wild-type E gene replaced by the TC-tagged form. The recombinant virus was designated as MHV E-TC. When MHV E-TC infected 17Cl1 cells were labeled with Lumio™ Red, the red fluorescence colocalized with the signal from the 9410 antibody that recognizes the carboxy end of E (Fig. 5A). Colocalization with the anti-E antibody demonstrated specificity of the Lumio™ Red staining in the infected cells. The E-TC virus did produce smaller plaques and growth kinetic

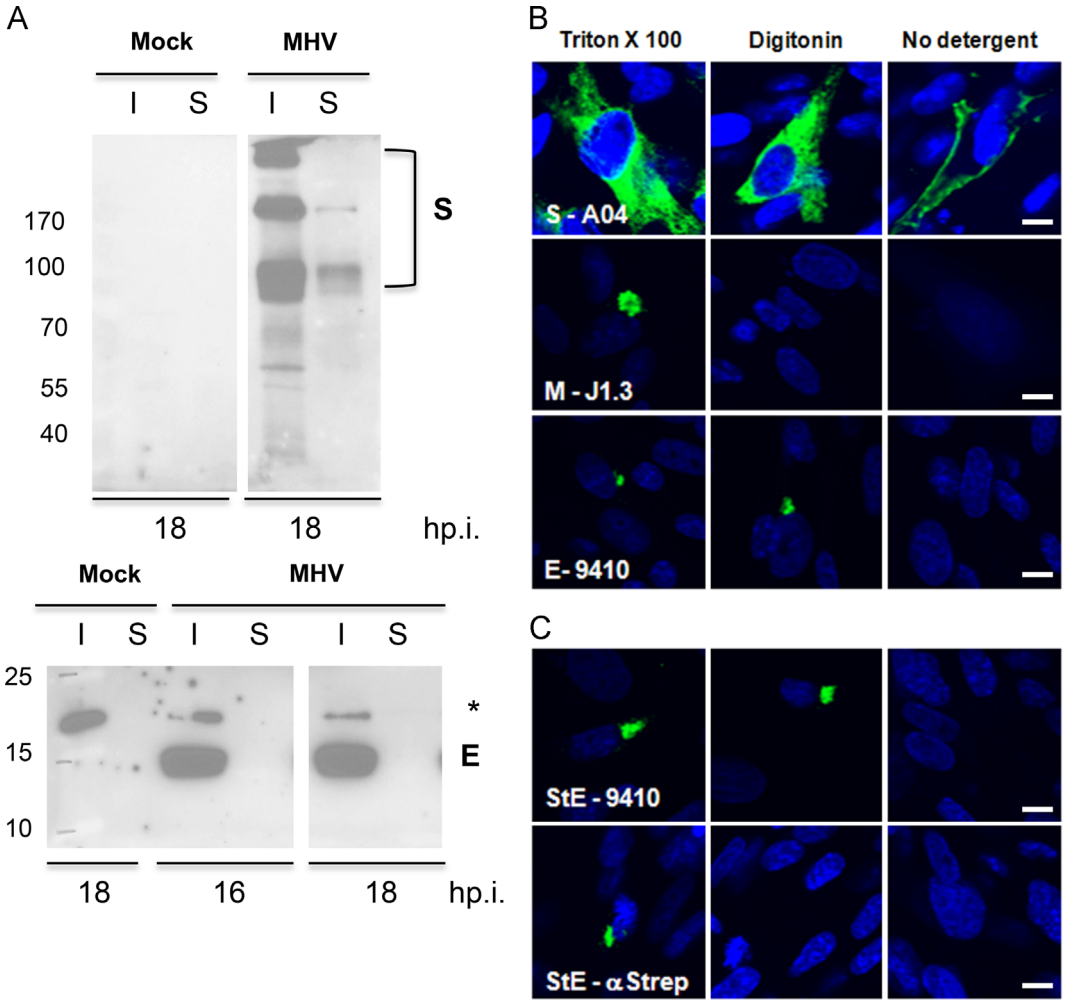

Fig. 3. MHV E does not traffic to the cell surface. (A) 17Cl1 cells were infected with MHV at an MOI of 0.1. At 16 & 18 h p.i., surface proteins were biotinylated. Surface (S) and intracellular (I) proteins were analyzed for spike (S) and envelope (E) proteins by Western blotting. For the analysis 10% and 20% of the intracellular and surface fractions, respectively were loaded. The Western blot for the E protein was exposed 15 × longer than that for the S protein. (B) 17Cl1 mouse cells were infected with MHV at an MOI of 0.1 (top three panels) and probed with antibodies specific for S, M and E after cells were permeabilized with digitonin or TX-100 to reveal the cytoplasmic or both luminal and cytoplasmic epitope of the protein. (C) BHK-21 cells were transfected with pCAGGS vector expressing MHV E with a Strep- tag at the amino end. The amino and carboxy ends of E were detected with an anti-Strep monoclonal, *Strep*MAB-Classic and rabbit anti-E 9410 antibodies, respectively. Scale bar, 5 μm.

analysis showed that the virus grew slower, yielding titers that were ~100-fold less than the WT untagged virus by 20 h p.i. (Fig. 5B). Nonetheless, sequencing and the continued presence of the TC tag, as indicated by fluorescence, demonstrated that the E-TC virus was stable through five passages. This indicated that MHV E-TC was replication- and assembly-competent and thus, a good model to study the dynamics of the protein in live cells.

Live-cell imaging of E protein in infected cells

The MHV E-TC virus allowed us to use live cell imaging to monitor the E protein during infection in mouse 17Cl1 cells. At 6 h p.i. Lumio™ Green was added to the medium and cells, maintained in an environmentally controlled chamber, were analyzed by confocal microscopy. Over the $t=0$–180 min timecourse the E protein remained at intracellular membranes and did not traffic to the cell surface, consistent with its localization in ERGIC/Golgi compartments (Fig. 6A).

To analyze the extent of mobility at the site of localization, FRAP (fluorescence recovery after photobleaching) was performed on MHV E-TC infected 17Cl1 cells at 8 h p.i. A region of interest (ROI) in the perinuclear area expressing E-TC was photobleached and recovery of fluorescence was monitored over a 300 s timecourse by confocal microscopy (Fig. 6B). The mobile fraction (M_f), the fraction of molecules capable of diffusing into the bleached ROI, was calculated from measurements taken from cells ($n=14$) in multiple experiments (Fig. 6C). The recovery ranged from 41% to 87%, with an average mobility fraction (M_f) of 61% ± 0.14, indicating that E is free to move within ERGIC/Golgi membranes. Four different recovery trends were observed in the infected cells ($n=14$) (Fig. 6D). Examples of the recovery trends (T2C5, T2C10, T3C5, T3C7), along with the corresponding images pre and post, are shown (Fig. 5B and D). While the mobility fraction revealed that the E protein was mobile, the rate of recovery was wide, ranging from 10 s to 200 s (Fig. 6E).

Correlative light electron microscopy of E protein in infected cells

Availability of a TC tag allows proteins to be imaged directly in live cells, as described above, but it also offers the advantage that cells can be analyzed by electron microscopy (EM) following addition of diaminobenzidine (DAB) and photoconversion. Cells infected with MHV E-TC were initially viewed by confocal microscopy after addition of Lumio™ Red (Fig. 7A). Photoexcitation of the Lumio™ Red reagent bound to a TC tag results in release of singlet oxygen, which in turn polymerizes added diaminobenzidine (DAB). The precipitate that forms can be visualized directly by EM following

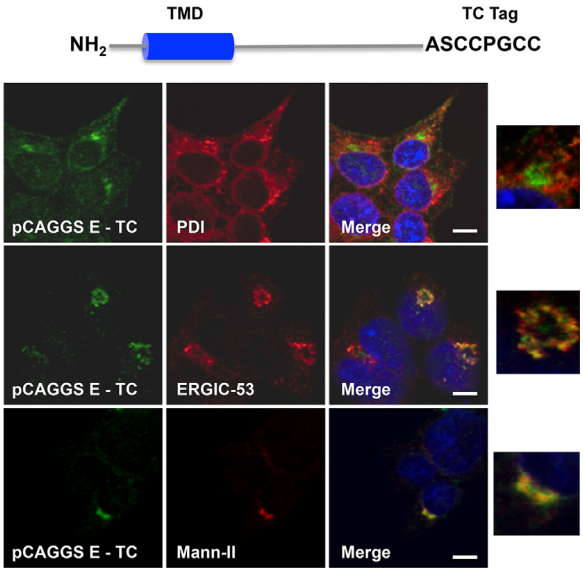

Fig. 4. Characterization of TC-tagged E. The schematic illustrates the location of TC tag at the carboxy ends of WT E. 293T cells were transfected with pCAGGS E-TC, fixed at 8 h posttransfection and processed for immunofluorescence to detect E using Lumio™ Green (left images), and ER, ERGIC or Golgi (red) markers (middle images). Yellow in the merged images indicates colocalization of signals. Enlarged inserts of selected cells are shown at the far right. Scale bar, 5 μm.

osmimum tetroxide staining. In MHV E-TC virus infected cells a precipitate was visible that colocalized with the Lumio™ Red labeling, as expected in a perinuclear position, consistent with the ERGIC/Golgi localization described earlier (Fig. 5A). When examined by EM the electron-dense precipitate was localized in Golgi stacks (Fig. 7B). In some cells Golgi fragmentation was evident and E was associated with ~20-nm vesicles, apparently derived from the stacks (data not shown).

Discussion

Coronavirus E proteins are clearly important for virus assembly and egress, but their mechanistic role(s) is still not understood. Genetic approaches have been used to examine contributions of various conserved residues and domains to gain insight about the function of the protein. Many of the alterations significantly impact virus production and transport out of the cell (Boscarino et al., 2008; Fischer et al., 1998; Kuo and Masters, 2003; Lopez et al., 2008; Ruch and Machamer, 2011; Ye and Hogue, 2007). E proteins from other coronaviruses can substitute for MHV E (Kuo et al., 2007). Recent studies demonstrated that SARS E protein is a virulence factor (DeDiego et al., 2011, 2014). Several studies have shown that SARS E protein interacts with cellular proteins, some of which likely participate in the functional roles that the protein plays (Alvarez et al., 2010; Jimenez-Guardeno et al., 2014; Teoh et al., 2010).

Earlier work concluded that MHV E accumulates in pre-Golgi membranes, based on colocalization with Rab-1, a marker characteristic of ER and ERGIC compartments, in electron-dense convoluted membrane structures (Raamsman et al., 2000). Our confocal imaging, in parallel with a full panel of exocytic pathway cellular markers, clearly shows that MHV E is not in the ER, but is present in both the ERGIC and Golgi, primarily in the *cis* and medial cisternae of the latter, early during infection. Based on the apparent similar roles that the E proteins play in virus assembly, it stands to reason that they likely share common localization characteristics. IBV and SARS-CoV E proteins were previously reported to localize in the ER and/or Golgi (Corse and Machamer, 2000; Liao et al., 2006; Lim and Liu, 2001; Nal et al., 2005). Recent studies have shown that SARS-CoV E colocalizes with ERGIC-53 in infected cells and also when expressed transiently (Nieto-Torres et al., 2011; Teoh et al., 2010). Strong transient expression of SARS-CoV E in the *cis*-Golgi, but hardly any expression in the ERGIC and trans-Golgi was also recently reported (Cohen et al., 2011; Nieto-Torres et al., 2011; Teoh et al., 2010). We previously showed as well that HA-tagged SARS-CoV E localized in both the ERGIC and Golgi during transient expression (Lopez et al., 2006). Collectively, it can be concluded that coronavirus E proteins are expressed in both ERGIC and Golgi compartments, though the distribution may vary depending on the virus and cell type.

Previous studies reported that coronavirus E proteins traffic to the cell surface (Godet et al., 1992; Yu et al., 1994; Yuan et al., 2006). In addition to surface immunofluorescence, cellular permeabilization by E proteins and whole-cell patch clamp measurement of ion channel activity in cells expressing SARS-CoV E were suggestive of surface expression (Liao et al., 2004, 2006; Madan

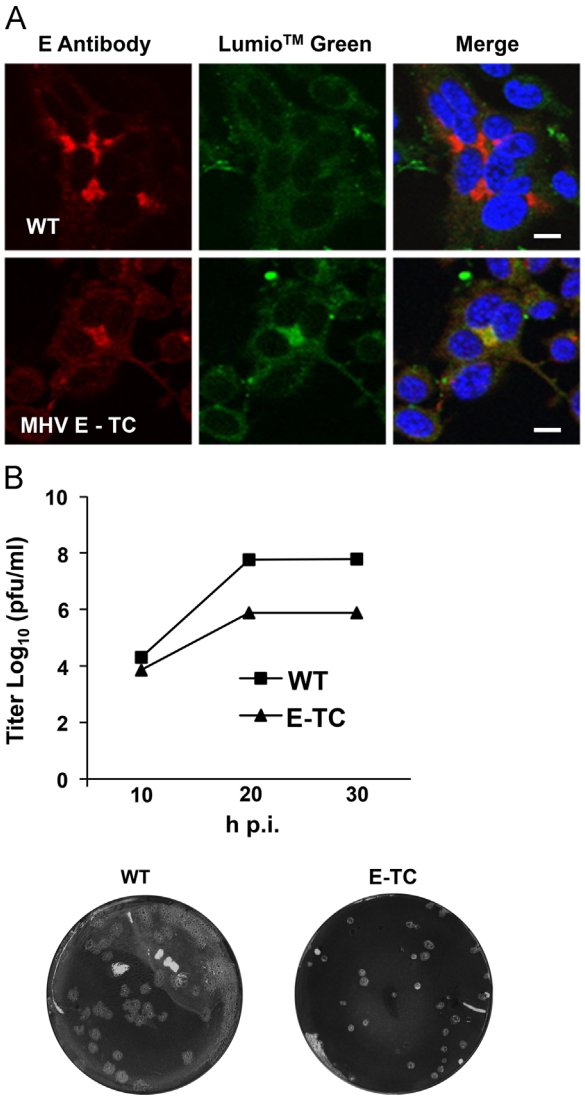

Fig. 5. MHV recombinant with TC-tagged E. (A) 17Cl1 mouse cells were infected with WT or MHV E-TC viruses at a MOI of 1. Cells were labeled with Lumio Green™ at 8 h p.i., fixed and stained for E with antibody 9410. Yellow in the merged panels indicates colocalization of TC-Lumio™ Green and E. (B) Growth kinetics and plaque characteristics of WT and MHV E-TC viruses were analyzed in 17Cl1 cells infected at a MOI of 0.01. Titers were determined by plaque assay on L2 cells at the indicated times. Growth kinetic titers represent the average of two independent experiments from plaque assays performed in duplicate. Scale bar, 5 μm.

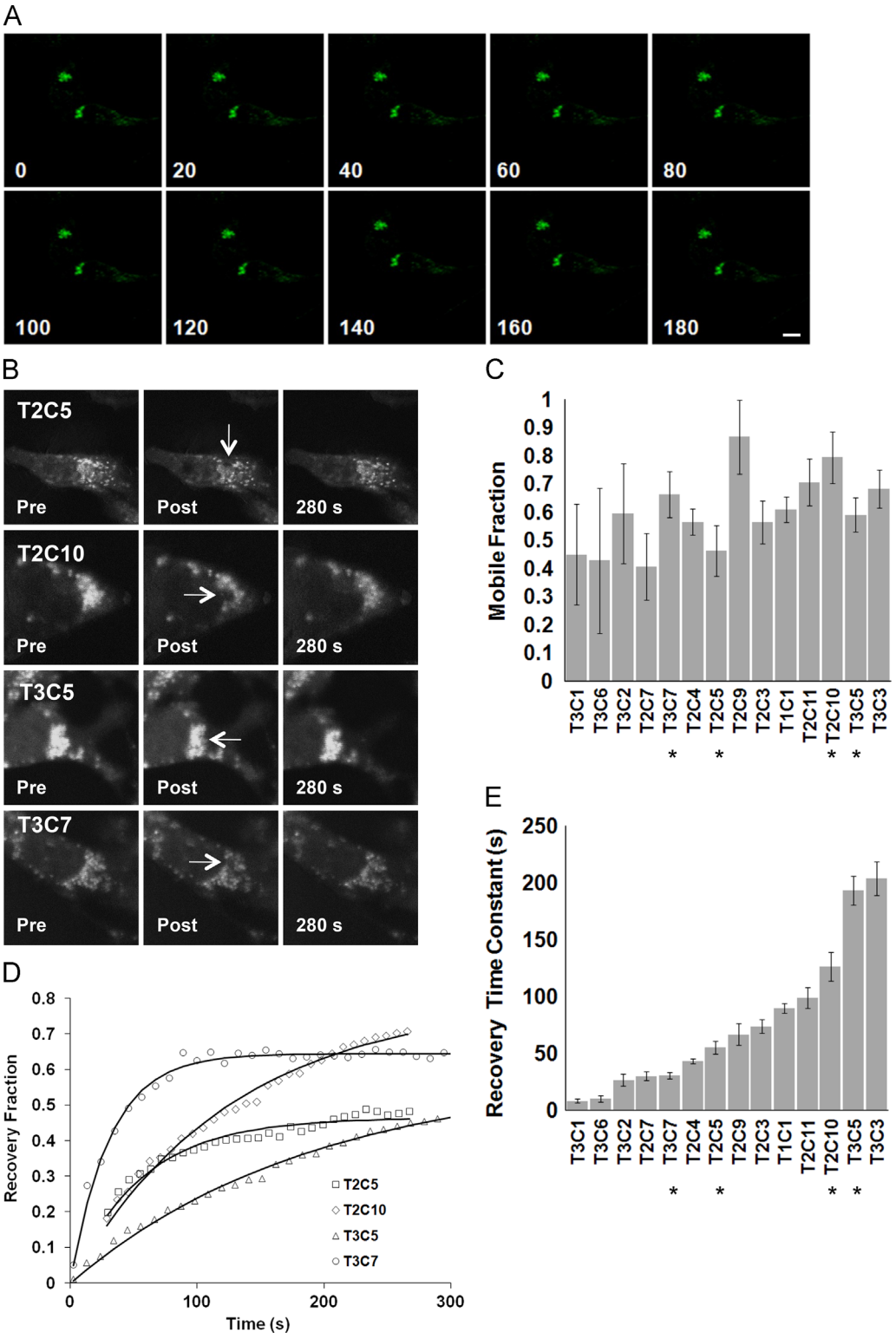

Fig. 6. Dynamics of TC-tagged E in infected cells. (A) Mouse 17Cl1 cells were infected with MHV E-TC at a MOI of 1. At 8 h p.i. cells were treated with Lumio™ Green. (A) Live cells were examined by confocal microscopy and images were collected at 20 min intervals over a 180 min time course with a *Z*-section setting of 0.5 μm. (B) FRAP was performed after treatment of infected cells with Lumio™ Green. Selected regions of interest were bleached and fluorescence recovery was monitored every 10 s over a ~300 s time course. Representative images from four cells are shown before and after photobleaching, bleached area indicated by arrows. (C) Fluorescence intensities (normalized to prebleach values) are shown plotted against time and the calculated mobile fractions (M_f) are indicated for each cell ($n=14$). Error bars indicate standard deviations from the mean. (D) Recovery fractions for the cells shown in B are plotted over the 300 s following photobleaching. (E) Recovery time constants for individual cells are shown. Asterisks in panels C and D indicate results from corresponding cells in panel B. FRAP images from 14 cells were analyzed from three independent experiments. Scale bar in A, 5 μm.

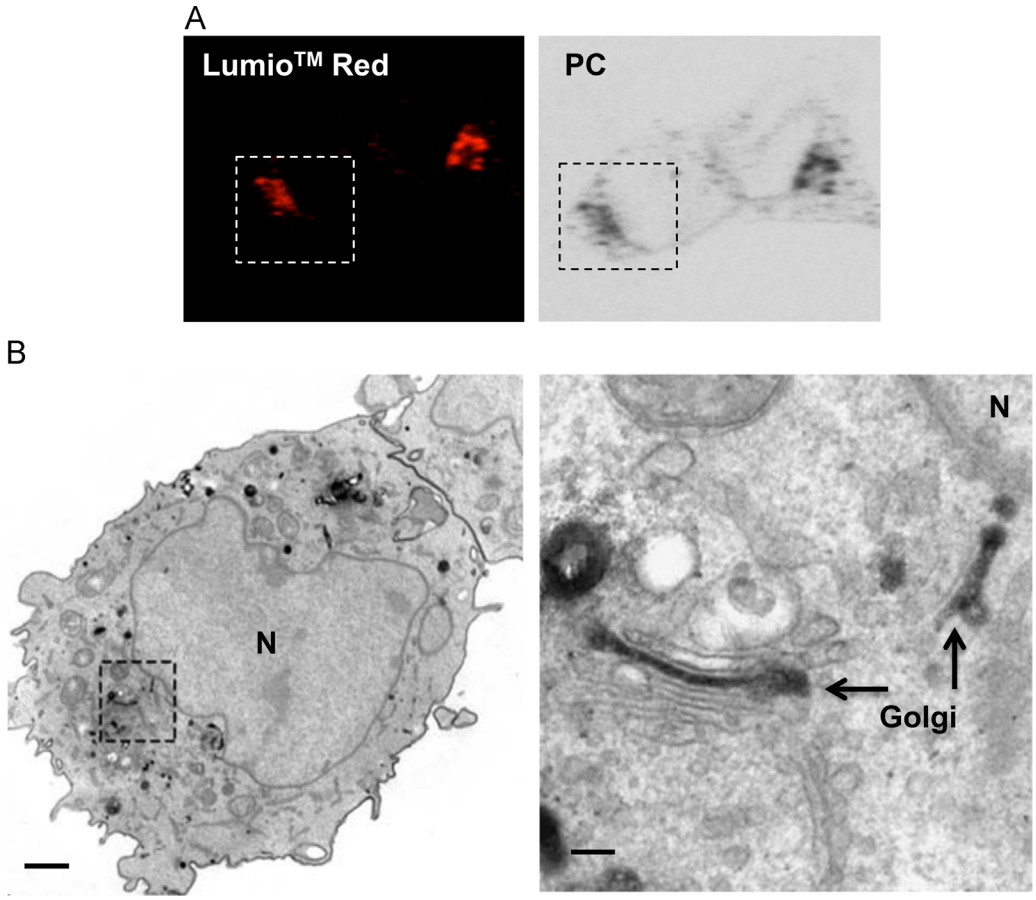

Fig. 7. CLEM of TC-tagged E in infected cells. Mouse 17Cl1 cells were infected with MHV E-TC virus at a MOI of 1. (A) At 8 h p.i. cells were stained with Lumio™ Red (left), followed by photoconversion (PC, right). (B) A low-magnification electron micrograph of the boxed cell in A is shown after photoconversion. The electron dense region corresponding to the Golgi region is boxed. A higher magnification shows electron density in Golgi stacks indicated by the arrows adjacent to the nucleus (N). Scale bars, 1 μm and 50 nm, respectively, for images in B.

et al., 2005; Pervushin et al., 2009). We did not detect MHV E on the surface of nonpermeabilized transfected or infected cells. This is consistent with the recent report which clearly demonstrated that SARS-CoV E is not present at the plasma membrane (Nieto-Torres et al., 2011). Our confocal microscopy analysis over a time course following infection strongly illustrates that E remains in its perinuclear location even late during infection. Results from our live-cell and CLEM imaging also support the conclusion that MHV E remains at the site of assembly in ERGIC/Golgi membranes and does not transport to the plasma membrane. Our surface expression results yielded additional information confirming that MHV E assumes an orientation with the amino end located in the lumen and the cytoplasmic tail in the cytoplasm, consistent with the recently described topology of SARS-CoV E (Nieto-Torres et al., 2011). The cytoplasmic tail of MHV E was previously determined to reside in the cytoplasm in infected cells and thus, outside of the virion, but with a FLAG tag placed at the amino end it was suggested that the protein spans the lipid bilayer twice with both the amino and carboxy ends in the cytoplasm (Maeda et al., 2001; Raamsman et al., 2000). Our results clearly show that the amino-terminal Strep tag does not alter the single pass topology with a luminal amino end and cytoplasmic carboxy end in the cellular membranes.

Live-cell imaging was only recently used to follow trafficking and dynamics of coronavirus proteins. Fluorescent tags such as GFP or mCherry were appended to nsp2, nsp4 or N proteins to study replication–transcription complexes and their relationship to formation of membrane structures in virus-infected cells (Freeman et al., 2014; Hagemeijer et al., 2011, 2010; Verheije et al., 2010). Results from our live cell imaging and FRAP analysis of MHV E-TC show that TC tagged E is mobile at internal membranes of infected 17Cl1 cells. Its average mobility (M_f=61%) is similar to what was measured for nsp4 in ER membranes (Hagemeijer et al., 2011). Nsp4 is a nonstructural integral membrane protein that localizes to the ER, but the protein is recruited during infection to replication complex structures that are interconnected with ER membranes, where its mobility (M_f=33%) is apparently restricted (Hagemeijer et al., 2011). The mobility of GFP tagged N and nsp2, both soluble cytoplasmic proteins, was also analyzed in cells infected with recombinant MHVs expressing the tagged constructs (Verheije et al., 2010; Hagemeijer et al., 2010). The N protein (M_f=40.4%) is dynamically associated with replication–transcription complexes, whereas nsp2 (M_f=9.9%) is thought to be immobilized through protein–protein interactions in the complexes in infected cells.

The E protein actually displayed a range of mobilities (M_f= 41–87%) at 6 h p.i., the point at which virus assembly is actively ongoing. Several factors may account for the M_f range. The population of E molecules that are actively involved in assembly maybe associated with other structural proteins or possibly host factors that differently restrict lateral diffusion in membranes. The E protein assembles into oligomeric ion channels that could affect the proteins mobility. Possibly only a fraction of molecules exists as part of a channel at any given time. The E protein is palmitoylated (Boscarino et al., 2008; Lopez et al., 2008). We do not know if all potential cysteine residues are modified at the same time or if possibly the protein undergoes dynamic palmitoylation/depalmitoylation cycling during infection. The conserved cysteines are located adjacent to the transmembrane domain, which when palmitoylated may influence

interaction of the protein tail with membranes and thus, its mobility. The HA protein of influenza virus is a transmembrane protein that is both palmitoylation and myristoylated. Yellow fluorescent protein (YFP) tagged HA exhibits different diffusion coefficients that vary based on the acylation state of the protein. WT HA-YFP has a diffusion coefficient of 0.14 $\mu m/s^2$ while a non-acylated mutant has a diffusion coefficient of 0.30 $\mu m/s^2$. The acylation greatly reduces the mobility of the protein (Engel et al., 2010). Depending on the number of sites that are palmitoylated, this may affect the mobility of E molecules. If E plays a role in membrane curvature or in scission, lateral movement of the protein in membranes at the site of assembly could facilitate the budding process. This might also contribute to the range of mobilities observed in this study.

Fluorescently labeled SARS-CoV structural proteins were also expressed previously to study VLP production and trafficking in live cells (Siu et al., 2008). VLPs were assembled with chimeric N and S proteins containing a fluorescent protein (cyan – eCFP or green – eGFP) tag fused at their carboxy termini, but similarly tagged M protein could not be incorporated. Data was not shown, but the authors indicated that the E protein did not tolerate addition of the large fluorescent protein tags (Siu et al., 2008). Our study highlights the potential utility and tolerance of the smaller TC tag since we were able to generate a recombinant virus with the tag fused to the carboxy end of E. The recombinant virus produced smaller plaques and reached titers of only 1×10^6 PFU/ml, compared with wild-type MHV A59 that generally yields titers in the range of 1×10^7–1×10^8 PFU/ml. Nonetheless, virus stability over multiple passages provides the opportunity to use the tagged virus for live cell studies. When the E gene is deleted or knocked out from MHV a small plaque phenotype and titers at least three orders of magnitude lower than the wild-type virus are produced (Kuo et al., 2007; Kuo and Masters, 2003). Thus, the virus with the TC-tagged E grows better than the E-null virus.

Assembly of coronaviruses at intracellular ERGIC membranes was established sometime ago (Klumperman et al., 1994; Krijnse-Locker et al., 1994; Tooze et al., 1984; Ulasli et al., 2010). More extensive and higher resolution views of ultrastructural changes that occur during replication and assembly were recently described (Ulasli et al., 2010). Three membranous structures, including large virion-containing vacuoles (LVCVs), tubular bodies (TBs) and cubic membrane structures (CMSs), were associated with virus assembly/release. The E protein was present with two of these structures, the LVCVs that are derived from ERGIC/Golgi membranes and TBs thought to form late in infection as a result of excess protein self-aggregation (Raamsman et al., 2000; Ulasli et al., 2010). The latter are thought to be equivalent to previously described smooth tubular membranous structures that are induced by E protein expression late during coronavirus infection (Raamsman et al., 2000). During the time frame in which our CLEM studies were conducted, we did not detect these tubular structures. It is possible that the lower yield of the E-TC virus might account for this. We did find E associated with Golgi cisternae and in some cells association with Golgi fragmentation was noted. Golgi fragmentation has been observed by confocal microscopy in cells infected with MHV or TGEV and also when IBV E was overexpressed (Lavi et al., 1996; Ortego et al., 2007; Ruch and Machamer, 2011; Ulasli et al., 2010). Golgi disruption was not observed in cells infected with a recombinant TGEV lacking the E gene, but fragmentation occurred when E was provided in *trans*, thus providing strong support for contribution of the protein to this process (Ortego et al., 2007). Our CLEM results illustrate the potential to follow E during infection and to monitor changes at the ultrastructural level that are associated with the protein, a direction that will be pursued further in future studies.

The accumulation of E in ERGIC/Golgi membranes and the fact that only a few molecules are incorporated into virions suggest that E likely provides a function(s) that is peripheral to or limited at most in the area where virion particles bud. Lack of E trafficking to the cell surface during infection lends additional support for the protein's participation in virus assembly and morphogenesis and possible other roles during infection from its position in the internal membranes. At these membranes E may through its ion channel transport of cations directly influence the immediate microenvironment in the ERGIC lumen by alteration of Na+ or K+ or other ion concentrations that could in turn result in luminal pH changes that are balanced by activation of vacuolar H^+ATPase. The ERGIC does contain an active H^+ ATPase that has been suggested to be possibly involved in directional transport and concentration of cargo molecules (Ying et al., 2000). A second, previously suggested, possibility is that E plays a role in helping mediate membrane curvature or scission (Vennema et al., 1996). Influenza M2, a well characterized multifunctional small integral membrane protein with proton-selective ion channel activity, plays a significant role in entry during infection, but it is also involved in virus assembly (Chen et al., 2008; Iwatsuki-Horimoto et al., 2006; McCown and Pekosz, 2006; Pinto and Lamb, 2006). Recently M2 was shown to mediate membrane curvature and scission during budding (Rossman et al., 2010). Coronavirus E proteins could play a similar role. Thirdly, coronavirus E proteins may through interactions with host proteins facilitate virus budding or vesicular transport. A large number of host proteins copurify with SARS virions and recently host and viral proteins that interact with E were identified (Alvarez et al., 2010; Neuman et al., 2008; Teoh et al., 2010). Finally, E ion channel activity at internal membranes may result in signaling that activates ion channel activity at the cell surface. While the latter is only speculative at this point, measurement of ion channel activity at the surface of cells expressing SARS-CoV E might reflect a response to such signaling and while such activity might be less likely to play a role in virus assembly and transport of LVCVs, such activity could impact a role of the protein as a virulence factor during infection (DeDiego et al., 2007, 2008; Pervushin et al., 2009; Teoh et al., 2010). SARS-CoV lacking the E gene is attenuated in animal models, thus the protein, at least for this virus, is a virulence factor (DeDiego et al., 2007, 2008; Netland et al., 2010). Recent results indicate that ion channel activity is an important contributor to virulence (DeDiego et al., 2014; Nieto-Torres et al., 2011). Thus, there are a large number of potential functions for the E protein which makes it an attractive target for antiviral therapeutic development.

Evidence for disruption of protein trafficking by overexpression of IBV E or during MHV infection has been described (Ruch and Machamer, 2011, 2012b). It is clear that E protein residence in the ERGIC/Golgi region impacts the local cellular environment, which may be linked to possibly multiple roles that it plays in virus assembly/release, as well as pathogenesis. The ability to monitor E directly in live cells and to extend this to ultrastructural studies using CLEM should expand the opportunities to analyze interactions between the protein and the cell during infection to help increase our understanding of its role(s) and mechanistically how it functions.

Materials and methods

Cells and viruses

Mouse 17 clone 1 (17Cl1) and L2, baby hamster kidney (BHK-21) and human 293T cells were maintained as previously described (Arndt et al., 2010). Wild type (WT) and recombinant MHV A59 virus stocks were grown in 17Cl1 cells at specified multiplicities of infection (MOI) and virus titers were determined in L2 cells.

Generation of TC-tagged E proteins

MHV E and tagged forms of the gene were expressed in the pCAGGS vector under the control of the chicken β-actin promoter

as described previously (Lopez et al., 2008). pCAGGS E-TC was constructed by PCR amplification using pCAGGS E as the template and appropriate primers that included the coding sequence for the tetracysteine tag (CCPGCC) and two preceding codons for alanine and serine.

Construction of recombinant MHV with TC tagged E

Recombinant MHV E-TC was made by reverse genetics using a MHV A59 clone (Yount et al., 2002). The coding sequence for WT E was replaced in the G clone with TC-tagged E as described above by three-way ligation of PCR amplified fragments covering the E gene locus and flanking regions. Following sequence confirmation of the subcloned region between *Sbf* I and *Nde* I restriction sites and junctions after ligation into the G clone, a full-length cDNA genomic clone was assembled, transcribed and electroporated into BHK-MHVR cells as described previously (Verma et al., 2006). Viruses were recovered, plaque purified, passaged and stability of the TC tag was confirmed after at least five passages.

Immunofluorescence

Mouse 17Cl1, hamster BHK-21 or human 293T cells were plated either on Nunc Lab-Tek chamber slides or coverslips (No. 1.5) in multiwell plates 1 day prior to use. Cells were infected at the specified MOIs or transfected using *Trans*IT-LT1 transfection reagent (MirusBio LLC, Madison, WI). At the specified times cells were washed with phosphate-buffered saline (PBS) and fixed with 100% methanol for 15 min at −20 °C for internal staining. Cells were washed with PBS and blocked with 0.2% gelatin in PBS for 1 h at room temperature (RT) or overnight at 4 °C. For surface staining cells were washed two times with PBS and fixed in freshly prepared 3% paraformaldehyde in PBS for 15 min at RT, followed by quenching with 10 mM glycine for 15 min. Cells were permeabilized with 0.1% Triton X-100 in PBS for 3 min for parallel internal staining, followed by washing and blocking with gelatin as described above. For digitonin permeabilization, cell chamber slides were placed on ice and rinsed in KHM buffer containing 110 mM potassium acetate, 20 mM HEPES (pH 7.2) and 2 mM magnesium acetate. Cells were permeabilized with 25 μg/ml of digitonin in KHM buffer on ice for 5 min, followed by two washes in PBS. Cells were fixed in 3% paraformaldehyde and quenched as described above.

Cells were incubated with appropriate primary antibodies for 2 h at RT, washed multiple times with 0.2% gelatin in PBS before incubation with AlexaFluor-labeled secondary antibodies (Invitrogen). Cells were washed several times in PBS containing 0.2% gelatin, once with PBS alone and mounted in ProLong Gold antifade reagent (Invitrogen). In most cases nuclei were stained with 4,6-diamino-2-phenylindole (DAPI) prior to mounting. Images were viewed using an epifluorescence Nikon inverted microscope (Nikon Inc., Melville, NY) with MetaMorph imaging software (Universal Imaging Corporation, Downingtown, PA). Image processing was performed using Adobe Photoshop. Laser scanning confocal microscopy was done using the Zeiss LSM 510 META microscope and software (Carl Zeiss, Inc., Thornwood, NY). Images were processed using Image J software (http://imagej.nih.gov/ij/).

Primary antibodies used in this study included rabbit polyclonal 9410 generated in the Hogue Lab against the carboxy terminal 21 amino acids of MHV E coupled to keyhole limpet hemocyanin (KLH). Mouse monoclonals J1.3 and 2.7 were previously described (Fleming et al., 1989) and polyclonal antibody A04 against MHV S was kindly provided by Kathryn Holmes, University of Colorado Health Sciences. Cells were processed for dual-label immunofluorescence detection with E using protein disulfide isomerase (PDI) (Alexis), ERGIC-53(Alexis), or mannosidase II (Mann-II) (Covance), as ER, ERGIC, and Golgi markers, respectively. Monoclonal antibody *Strep*MAB-Classic (IBA) was used to detect the *Strep* tag appended to the E protein.

Biotinylation of surface proteins

Mouse 17Cl1 cells were plated on 60 mm cell culture dishes (BD Biosciences) 1 day prior to use. Cells were infected at a MOI of 0.1. At 8, 12 and 16 h p.i. the media were aspirated and cells were washed twice in PBS. Cells were incubated on ice with 1 mg/ml biotin (Thermo Fisher Scientific) for 1 h. Cells were washed twice in PBS and biotin was quenched with 50 mM glycine in PBS for 5 min. Cells were lysed in biotinylation lysis buffer containing 10 mM HEPES (pH 7.2), 0.2% NP-40, 150 mM NaCl containing protease inhibitor cocktail (Sigma, St. Louis, MO) at 0 °C for 10 min. Lysates were clarified at 16,000 × *g* for 10 min at 4 °C. Streptavidin agarose resin (ThermoFisher Scientific) was equilibrated in biotinylation lysis buffer and added to the cell lysate. Binding was carried out at 4 °C with constant rotation. The Streptavidin agarose resin was pelleted at 4000 × *g* for 10 min at 4 °C. Biotinylated surface proteins were eluted from the agarose resin in Laemmli sample buffer by heating at 100 °C. 10% of the intracellular fraction and 40% of the surface fraction were loaded onto SDS-PAGE gels and subsequently analyzed by Western blotting.

Live cell imaging

Mouse 17Cl1 cells were grown in glass bottom 35 mm dishes (MatTek) and subsequently infected at a MOI of 0.1 with MHV E-TC virus. At 7 h p.i. cells were washed in serum free Opti-MEM and labeled with 200 nM Lumio™ Green (FlAsH™) reagent (Invitrogen) in Opti-MEM for 30 min at 37 °C in the presence of CO_2. Cells were washed thoroughly with Opti- MEM, refed with 1X MEM without phenol red, plus 200 nM disperse blue for background reduction and allowed to recover for 30 min at 37 °C. Cells were monitored and imaged using a Zeiss LSM 510 META Confocal Microscope with the 488 nm laser at 5% power in a humidified chamber supplied with CO_2 and equipped with a heated stage and objective. Images were captured every 10 min over a 3 h 20 min timecourse with *Z*-sections of 0.5 μm.

Fluorescence recovery after photobleaching (FRAP)

Mouse 17Cl1 cells were grown in glass bottom 35 mm dishes (MatTek) and infected with MHV E-TC virus at a MOI of 0.1 pfu/cell. Cells were stained with 200 nM Lumio™ Green (FlAsH™) reagent (Invitrogen) and imaged as described above. Individual cells were selected for FRAP analysis. Selected regions were photobleached with a 488 nm laser at 100% power and recovery was measured every 5 s for 5 min. Initial signal intensity was set as 100% and signal recovery was calculated accordingly. Mobility fraction was calculated as the percentage of fluorescence recovery from what was measured immediately following photobleaching.

Correlative light electron microscopy (CLEM)

Mouse 17Cl1 cells were grown on 35 mm gridded glass bottom dishes (MatTek). Cells were infected with MHV E-TC virus at a MOI of 0.5 pfu/cell. At 8 h p.i. cells were washed twice with Opti-MEM and labeled with 200 nM Lumio™ Red (ReAsH™) reagent (Invitrogen) in Opti-MEM. Cells were incubated for 30 min in the presence of CO_2. After washing, cells were refed with Opti-MEM containing 0.5 μM 2,3-dimercapto-1-propanol plus 20 mM DTT and incubated in the presence of CO_2 for an additional 30 min. Cells were washed to remove all traces of DTT and refed with 1 ml of 1:1 DMEM:Opti-MEM containing 2.5% fetal calf serum. Cell images were collected using a Zeiss LMS 510 META Confocal Microscope.

For photoconversion after labeling with Lumio™ Red, cells were fixed with 2% glutaraldehyde in 100 mM sodium cacodylate buffer (pH 7.4) and incubated for 30 min at 37 °C. Cells were rinsed in 100 mM cacodylate buffer and treated for 5 min with blocking buffer (100 mM cacodylate buffer (pH 7.4) supplemented with 10 mM potassium cyanide, 10 mM aminotriazole, 0.01% hydrogen peroxide and 50 mM glycine). After rinsing with blocking buffer a solution of 1 mg/ml diaminobenzidine in 100 mM cacodylate buffer (pH 7.4) was added to cells. Photoconversion was performed using intense illumination (75 W xenon lamp without neutral density filters) focused through the 10 × microscope objective. Cells of interest for further electron microscopy analysis were identified by their location on the gridded coverslips.

Cells were washed with 0.1 M phosphate buffer (pH 7.4) before being fixed with a mixture of 1% osmium tetroxide and 0.8% potassium ferricyanide in distilled water for 1 h at 4 °C. Cells were stained with 2% uranyl acetate in water for 1 h and dehydrated through a series of increasing concentrations of acetone for 10 min each at RT. Resin infiltration with epoxy TAAB 812 (Electron Microscopy Sciences, Hatfield, PA) was carried out by increasing the resin to acetone ratio from 25% to 100% and polymerization at 60 °C for 48 h. Previously selected cells were sectioned at 70 nm and collected on formvar coated copper grids. Images were collected on a Philips 80 kV STEM microscope and processed using Image J software (http://imagej.nih.gov/ij/).

Acknowledgments

The work was supported by National Institutes of Health Grant AI53704 and in part by GM094599 funding for the ASU Center for Membrane Proteins in Infectious Diseases as part of the Protein Structure Initiative (PSI). LAL was supported in part by the American Society for Microbiology Robert D. Watkins Graduate Research Fellowship and KD was supported in part by a Science Foundation Arizona Graduate Research Fellowship. We thank Dr. Robert Roberson, David Lowry (Electron Microscopy Lab, Life Science Bioimaging Facility) and Douglas Daniel (Biodesign Confocal Microscopy) at ASU for helpful discussions and assistance with the microscopy and Dr. Henry H. Hogue for assistance with the FRAP data analysis.

References

Almazan, F., DeDiego, M.L., Sola, I., Zuniga, S., Nieto-Torres, J.L., Marquez-Jurado, S., Andres, G., Enjuanes, L., 2013. Engineering a replication-competent, propagation-defective Middle East respiratory syndrome coronavirus as a vaccine candidate. mBio 4, e00650–00613.

Alvarez, E., Dediego, M.L., Nieto-Torres, J.L., Jimenez-Guardeno, J.M., Marcos-Villar, L., Enjuanes, L., 2010. The envelope protein of severe acute respiratory syndrome coronavirus interacts with the non-structural protein 3 and is ubiquitinated. Virology 402, 281–291.

Arndt, A.L., Larson, B.J., Hogue, B.G., 2010. A conserved domain in the coronavirus membrane protein tail is important for virus assembly. J. Virol. 84, 11418–11428.

Boscarino, J.A., Logan, H.L., Lacny, J.J., Gallagher, T.M., 2008. Envelope protein palmitoylations are crucial for murine coronavirus assembly. J. Virol. 82, 2989–2999.

Chen, B.J., Leser, G.P., Jackson, D., Lamb, R.A., 2008. The influenza virus M2 protein cytoplasmic tail interacts with the M1 protein and influences virus assembly at the site of virus budding. J. Virol. 82, 10059–10070.

Cohen, J.R., Lin, L.D., Machamer, C.E., 2011. Identification of a Golgi complex-targeting signal in the cytoplasmic tail of the severe acute respiratory syndrome coronavirus envelope protein. J. Virol. 85, 5794–5803.

Corse, E., Machamer, C.E., 2000. Infectious bronchitis virus E protein is targeted to the Golgi complex and directs release of virus-like particles. J. Virol. 74, 4319–4326.

Corse, E., Machamer, C.E., 2002. The cytoplasmic tail of infectious bronchitis virus e protein directs Golgi targeting. J. Virol. 76, 1273–1284.

Curtis, K.M., Yount, B., Baric, R.S., 2002. Heterologous gene expression from transmissible gastroenteritis virus replicon particles. J. Virol. 76, 1422–1434.

DeDiego, M.L., Alvarez, E., Almazan, F., Rejas, M.T., Lamirande, E., Roberts, A., Shieh, W.J., Zaki, S.R., Subbarao, K., Enjuanes, L., 2007. A severe acute respiratory syndrome coronavirus that lacks the E gene is attenuated in vitro and in vivo. J. Virol. 81, 1701–1713.

DeDiego, M.L., Nieto-Torres, J.L., Jimenez-Guardeno, J.M., Regla-Nava, J.A., Alvarez, E., Oliveros, J.C., Zhao, J., Fett, C., Perlman, S., Enjuanes, L., 2011. Severe acute respiratory syndrome coronavirus envelope protein regulates cell stress response and apoptosis. PLoS Pathog. 7, e1002315.

DeDiego, M.L., Nieto-Torres, J.L., Jimenez-Guardeno, J.M., Regla-Nava, J.A., Castano-Rodriguez, C., Fernandez-Delgado, R., Usera, F., Enjuanes, L., 2014. Coronavirus virulence genes with main focus on SARS-CoV envelope gene. Virus Res 194, 124–137.

DeDiego, M.L., Pewe, L., Alvarez, E., Rejas, M.T., Perlman, S., Enjuanes, L., 2008. Pathogenicity of severe acute respiratory coronavirus deletion mutants in hACE-2 transgenic mice. Virology 376, 379–389.

Engel, S., Scolari, S., Thaa, B., Krebs, N., Korte, T., Herrmann, A., Veit, M., 2010. FLIM–FRET and FRAP reveal association of influenza virus haemagglutinin with membrane rafts. Biochem. J. 425, 567–573.

Fischer, F., Stegen, C.F., Masters, P.S., Samsonoff, W.A., 1998. Analysis of constructed E gene mutants of mouse hepatitis virus confirms a pivotal role for E protein in coronavirus assembly. J. Virol. 72, 7885–7894.

Fleming, J.O., Shubin, R.A., Sussman, M.A., Casteel, N., Stohlman, S.A., 1989. Monoclonal antibodies to the matrix (E1) glycoprotein of mouse hepatitis virus protect mice from encephalitis. Virology 168, 162–167.

Freeman, M.C., Graham, R.L., Lu, X., Peek, C.T., Denison, M.R., 2014. Coronavirus replicase-reporter fusions provide quantitative analysis of replication and replication complex formation. J. Virol. 88, 5319–5327.

Gaietta, G., Deerinck, T.J., Adams, S.R., Bouwer, J., Tour, O., Laird, D.W., Sosinsky, G.E., Tsien, R.Y., Ellisman, M.H., 2002. Multicolor and electron microscopic imaging of connexin trafficking. Science 296, 503–507.

Godet, M., L'Haridon, R., Vautherot, J.F., Laude, H., 1992. TGEV corona virus ORF4 encodes a membrane protein that is incorporated into virions. Virology 188, 666–675.

Griffin, B.A., Adams, S.R., Tsien, R.Y., 1998. Specific covalent labeling of recombinant protein molecules inside live cells. Science 281, 269–272.

Hagemeijer, M.C., Ulasli, M., Vonk, A., Reggiori, F., Rottier, P.J., de Haan, C.A., 2011. Mobility and interactions of the coronavirus nonstructural protein 4. J. Virol 85, 4572–4577.

Hagemeijer, M.C., Verheije, M.H., Ulasli, M., Shaltiel, I.A., de Vries, L.A., Reggiori, F., Rottier, P.J., de Haan, C.A., 2010. Dynamics of coronavirus replication–transcription complexes. J. Virol. 84, 2134–2149.

Heald-Sargent, T., Gallagher, T., 2012. Ready, set, fuse! The coronavirus spike protein and acquisition of fusion competence. Viruses 4, 557–580.

Hogue, B.G., Machamer, C.M., 2008. Coronavirus structural proteins and assembly. In: Perlman, S.G. (Ed.), The Nidoviruses. Amercan Society for Microbiology Press, Washington, DC, pp. 179–200.

Iwatsuki-Horimoto, K., Horimoto, T., Noda, T., Kiso, M., Maeda, J., Watanabe, S., Muramoto, Y., Fujii, K., Kawaoka, Y., 2006. The cytoplasmic tail of the influenza A virus M2 protein plays a role in viral assembly. J. Virol. 80, 5233–5240.

Jimenez-Guardeno, J.M., Nieto-Torres, J.L., DeDiego, M.L., Regla-Nava, J.A., Fernandez-Delgado, R., Castano-Rodriguez, C., Enjuanes, L., 2014. The PDZ-binding motif of severe acute respiratory syndrome coronavirus envelope protein is a determinant of viral pathogenesis. PLoS Pathog. 10, e1004320.

Klumperman, J., Locker, J.K., Meijer, A., Horzinek, M.C., Geuze, H.J., Rottier, P.J., 1994. Coronavirus M proteins accumulate in the Golgi complex beyond the site of virion budding. J. Virol. 68, 6523–6534.

Krijnse-Locker, J., Ericsson, M., Rottier, P.J., Griffiths, G., 1994. Characterization of the budding compartment of mouse hepatitis virus: evidence that transport from the RER to the Golgi complex requires only one vesicular transport step. J. Cell Biol. 124, 55–70.

Kuo, L., Hurst, K.R., Masters, P.S., 2007. Exceptional flexibility in the sequence requirements for coronavirus small envelope protein function. J. Virol. 81, 2249–2262.

Kuo, L., Masters, P.S., 2003. The small envelope protein E is not essential for murine coronavirus replication. J. Virol. 77, 4597–4608.

Kuo, L., Masters, P.S., 2010. Evolved variants of the membrane protein can partially replace the envelope protein in murine coronavirus assembly. J. Virol. 84, 12872–12885.

Lavi, E., Wang, Q., Weiss, S.R., Gonatas, N.K., 1996. Syncytia formation induced by coronavirus infection is associated with fragmentation and rearrangement of the Golgi apparatus. Virology 221, 325–334.

Liao, Y., Lescar, J., Tam, J.P., Liu, D.X., 2004. Expression of SARS-coronavirus envelope protein in *Escherichia coli* cells alters membrane permeability. Biochem. Biophys. Res. Commun. 325, 374–380.

Liao, Y., Yuan, Q., Torres, J., Tam, J.P., Liu, D.X., 2006. Biochemical and functional characterization of the membrane association and membrane permeabilizing activity of the severe acute respiratory syndrome coronavirus envelope protein. Virology 349, 264–275.

Lim, K.P., Liu, D.X., 2001. The missing link in coronavirus assembly. Retention of the avian coronavirus infectious bronchitis virus envelope protein in the pre-Golgi compartments and physical interaction between the envelope and membrane proteins. J. Biol. Chem. 276, 17515–17523.

Liu, D.X., Inglis, S.C., 1991. Association of the infectious bronchitis virus 3c protein with the virion envelope. Virology 185, 911–917.

Locker, J.K., Griffiths, G., Horzinek, M.C., Rottier, P.J., 1992. O-glycosylation of the coronavirus M protein. Differential localization of sialyltransferases in N- and O-linked glycosylation. J. Biol. Chem. 267, 14094–14101.

Lopez, L.A., Jones, A., Arndt, W.D., Hogue, B.G., 2006. Subcellular localization of SARS-CoV structural proteins. Adv. Exp. Med. Biol. 581, 297–300.

Lopez, L.A., Riffle, A.J., Pike, S.L., Gardner, D., Hogue, B.G., 2008. Importance of conserved cysteine residues in the coronavirus envelope protein. J. Virol. 82, 3000–3010.
Madan, V., Garcia, M.J., Sanz, M.A., Carrasco, L., 2005. Viroporin activity of murine hepatitis virus E protein. FEBS Lett. 579, 3607–3612.
Maeda, J., Repass, J.F., Maeda, A., Makino, S., 2001. Membrane topology of coronavirus E protein. Virology 281, 163–169.
McCown, M.F., Pekosz, A., 2006. Distinct domains of the influenza a virus M2 protein cytoplasmic tail mediate binding to the M1 protein and facilitate infectious virus production. J. Virol. 80, 8178–8189.
Nal, B., Chan, C., Kien, F., Siu, L., Tse, J., Chu, K., Kam, J., Staropoli, I., Crescenzo-Chaigne, B., Escriou, N., van der, W.S., Yuen, K.Y., Altmeyer, R., 2005. Differential maturation and subcellular localization of severe acute respiratory syndrome coronavirus surface proteins S, M and E. J. Gen. Virol. 86, 1423–1434.
Netland, J., Dediego, M.L., Zhao, J., Fett, C., Alvarez, E., Nieto-Torres, J.L., Enjuanes, L., Perlman, S., 2010. Immunization with an attenuated severe acute respiratory syndrome coronavirus deleted in E protein protects against lethal respiratory disease. Virology 399, 120–128.
Neuman, B.W., Joseph, J.S., Saikatendu, K.S., Serrano, P., Chatterjee, A., Johnson, M.A., Liao, L., Klaus, J.P., Yates III, J.R., Wuthrich, K., Stevens, R.C., Buchmeier, M.J., Kuhn, P., 2008. Proteomics analysis unravels the functional repertoire of coronavirus nonstructural protein 3. J. Virol. 82, 5279–5294.
Nieto-Torres, J.L., Dediego, M.L., Alvarez, E., Jimenez-Guardeno, J.M., Regla-Nava, J.A., Llorente, M., Kremer, L., Shuo, S., Enjuanes, L., 2011. Subcellular location and topology of severe acute respiratory syndrome coronavirus envelope protein. Virology 415, 69–82.
Ortego, J., Ceriani, J.E., Patino, C., Plana, J., Enjuanes, L., 2007. Absence of E protein arrests transmissible gastroenteritis coronavirus maturation in the secretory pathway. Virology 368, 296–308.
Ortego, J., Escors, D., Laude, H., Enjuanes, L., 2002. Generation of a replication-competent, propagation-deficient virus vector based on the transmissible gastroenteritis coronavirus genome. J. Virol. 76, 11518–11529.
Pervushin, K., Tan, E., Parthasarathy, K., Lin, X., Jiang, F.L., Yu, D., Vararattanavech, A., Soong, T.W., Liu, D.X., Torres, J., 2009. Structure and inhibition of the SARS coronavirus envelope protein ion channel. PLoS Pathog. 5, e1000511.
Pinto, L.H., Lamb, R.A., 2006. The M2 proton channels of influenza A and B viruses. J. Biol. Chem. 281, 8997–9000.
Raamsman, M.J., Locker, J.K., de Hooge, A., de Vries, A.A., Griffiths, G., Vennema, H., Rottier, P.J., 2000. Characterization of the coronavirus mouse hepatitis virus strain A59 small membrane protein E. J. Virol. 74, 2333–2342.
Regla-Nava, J.A., Nieto-Torres, J.L., Jimenez-Guardeno, J.M., Fernandez-Delgado, R., Fett, C., Castano-Rodriguez, C., Perlman, S., Enjuanes, L., DeDiego, M.L., 2015. SARS coronaviruses with mutations in E protein are attenuated and promising vaccine candidates. J. Virol. http://dx.doi.org/10.1128/JVI.03566-14 (in press).
Rossman, J.S., Jing, X., Leser, G.P., Lamb, R.A., 2010. Influenza virus M2 protein mediates ESCRT-independent membrane scission. Cell 142, 902–913.
Ruch, T.R., Machamer, C.E., 2011. The hydrophobic domain of infectious bronchitis virus E protein alters the host secretory pathway and is important for release of infectious virus. J. Virol. 85, 675–685.
Ruch, T.R., Machamer, C.E., 2012a. The coronavirus e protein: assembly and beyond. Viruses 4, 363–382.
Ruch, T.R., Machamer, C.E., 2012b. A single polar residue and distinct membrane topologies impact the function of the infectious bronchitis coronavirus E protein. PLoS Pathog. 8, e1002674.
Siu, Y.L., Teoh, K.T., Lo, J., Chan, C.M., Kien, F., Escriou, N., Tsao, S.W., Nicholls, J.M., Altmeyer, R., Peiris, J.S., Bruzzone, R., Nal, B., 2008. The M, E, and N structural proteins of the severe acute respiratory syndrome coronavirus are required for efficient assembly, trafficking, and release of virus-like particles. J. Virol. 82, 11318–11330.
Smith, A.R., Boursnell, M.E., Binns, M.M., Brown, T.D., Inglis, S.C., 1990. Identification of a new membrane-associated polypeptide specified by the coronavirus infectious bronchitis virus. J. Gen. Virol. 71 (Pt 1), 3–11.
Teoh, K.T., Siu, Y.L., Chan, W.L., Schluter, M.A., Liu, C.J., Peiris, J.S., Bruzzone, R., Margolis, B., Nal, B., 2010. The SARS coronavirus E protein interacts with PALS1 and alters tight junction formation and epithelial morphogenesis. Mol. Biol. Cell 21, 3838–3852.
Tooze, J., Tooze, S., Warren, G., 1984. Replication of coronavirus MHV-A59 in sac- cells: determination of the first site of budding of progeny virions. Eur. J. Cell Biol. 33, 281–293.
Tooze, J., Tooze, S.A., 1985. Infection of AtT20 murine pituitary tumour cells by mouse hepatitis virus strain A59: virus budding is restricted to the Golgi region. Eur. J. Cell Biol. 37, 203–212.
Ulasli, M., Verheije, M.H., de Haan, C.A., Reggiori, F., 2010. Qualitative and quantitative ultrastructural analysis of the membrane rearrangements induced by coronavirus. Cell. Microbiol. 12, 844–861.
Vennema, H., Godeke, G.J., Rossen, J.W., Voorhout, W.F., Horzinek, M.C., Opstelten, D.J., Rottier, P.J., 1996. Nucleocapsid-independent assembly of coronavirus-like particles by co-expression of viral envelope protein genes. EMBO J. 15, 2020–2028.
Verheije, M.H., Hagemeijer, M.C., Ulasli, M., Reggiori, F., Rottier, P.J., Masters, P.S., de Haan, C.A., 2010. The coronavirus nucleocapsid protein is dynamically associated with the replication–transcription complexes. J. Virol. 84, 11575–11579.
Verma, S., Bednar, V., Blount, A., Hogue, B.G., 2006. Identification of functionally important negatively charged residues in the carboxy end of mouse hepatitis coronavirus A59 nucleocapsid protein. J. Virol. 80, 4344–4355.
Wilson, L., Gage, P., Ewart, G., 2006. Hexamethylene amiloride blocks E protein ion channels and inhibits coronavirus replication. Virology 353, 294–306.
Wilson, L., McKinlay, C., Gage, P., Ewart, G., 2004. SARS coronavirus E protein forms cation-selective ion channels. Virology 330, 322–331.
Ye, Y., Hogue, B.G., 2007. Role of the coronavirus E viroporin protein transmembrane domain in virus assembly. J. Virol. 81, 3597–3607.
Ying, M., Flatmark, T., Saraste, J., 2000. The p58-positive pre-golgi intermediates consist of distinct subpopulations of particles that show differential binding of COPI and COPII coats and contain vacuolar H(+)-ATPase. J. Cell Sci. 113 (Pt 20), 3623–3638.
Yount, B., Denison, M.R., Weiss, S.R., Baric, R.S., 2002. Systematic assembly of a full-length infectious cDNA of mouse hepatitis virus strain A59. J. Virol. 76, 11065–11078.
Yu, X., Bi, W., Weiss, S.R., Leibowitz, J.L., 1994. Mouse hepatitis virus gene 5b protein is a new virion envelope protein. Virology 202, 1018–1023.
Yuan, Q., Liao, Y., Torres, J., Tam, J.P., Liu, D.X., 2006. Biochemical evidence for the presence of mixed membrane topologies of the severe acute respiratory syndrome coronavirus envelope protein expressed in mammalian cells. FEBS Lett. 580, 3192–3200.